MEDS Clinical Medicine (2025)
Clausius Scientific Press, Canada

DOI: 10.23977/medsc.2025.060417
ISSN 2616-1907 Vol. 6 Num. 4

Identification of Hypoxia-Related Biomarkers for Proliferative Diabetic Retinopathy: An Integrative Bioinformatics Analysis

Dingqiao Wang[1], Peidong Yuan[2], Hongzhi Yuan[2,*]

[1]Department of Ophthalmology, The Eighth Affiliated Hospital, Sun Yat-Sen University, Shenzhen, China
[2]Department of Ophthalmology, The Seventh Affiliated Hospital, Sun Yat-Sen University, Shenzhen, China
**Corresponding author: yuanhongzhi@sysush.com*

Keywords: Proliferative Diabetic Retinopathy, Hypoxia-Related Genes, CXCL9, DSC2, DSC3, PITRM1, Bioinformatics, Immune Infiltration

Abstract: Proliferative diabetic retinopathy (PDR) is a vision-threatening complication of diabetes, in which hypoxia plays a central pathogenic role. However, the hypoxia-associated molecular mechanisms and biomarkers in PDR remain incompletely understood. RNA sequencing data from patients with PDR and healthy controls (GSE146615) were analyzed to identify differentially expressed genes (DEGs). Hypoxia-related genes (HRGs) were obtained from the GeneCards database and integrated with DEGs and weighted gene co-expression network analysis (WGCNA) modules. Candidate genes were refined using least absolute shrinkage and selection operator (LASSO) regression and extreme gradient boosting (XGBoost). Diagnostic performance was assessed by receiver operating characteristic (ROC) analysis. Immune infiltration was estimated with the CIBERSORT algorithm, and biomarker–immune cell correlations were examined. We identified 1,650 DEGs in PDR, enriched in immune regulation, vascular function, and mitochondrial pathways. Intersection analysis identified 13 hypoxia-related genes, of which four—CXCL9, DSC2, DSC3, and PITRM1—were selected as key biomarkers by LASSO and XGBoost. ROC analysis showed strong diagnostic performance for PITRM1 (AUC = 0.863), DSC2 (AUC = 0.861), DSC3 (AUC = 0.837), and CXCL9 (AUC = 0.749). Immune infiltration analysis revealed increased plasma cells and $CD8^+$ T cells, and decreased resting mast cells in PDR. This integrative bioinformatics analysis identified four hypoxia-related genes as potential diagnostic biomarkers for PDR, providing insights into hypoxia-driven immune and vascular changes in disease pathogenesis. These findings may inform future diagnostic and therapeutic strategies.

1. Introduction

Diabetic retinopathy (DR) represents a prevalent microvascular complication of diabetes and a major cause of vision loss among working-age individuals worldwide. [1]. Proliferative diabetic

retinopathy (PDR), the most severe form of DR, is defined by abnormal retinal neovascularization and affects roughly 7% of individuals with diabetes globally [2]. With the continuous growth in diabetes incidence, PDR has become an increasingly important public health concern [3]. Despite the availability of treatments such as anti-VEGF agents and laser photocoagulation, PDR remains a leading contributor to vision loss, underscoring the pressing need to clarify its underlying pathogenic pathways and to discover new therapeutic opportunities [4].

The development of PDR is driven by a cascade of events initiated by hyperglycemia-induced retinal microvascular injury, progressing through vascular dysfunction, retinal ischemia, and ultimately uncontrolled neovascular growth [5]. Persistent hyperglycemia impairs retinal blood flow and oxygen delivery, generating localized ischemic and hypoxic conditions [6,7]. This low-oxygen environment activates hypoxia-inducible factors (HIFs), which in turn stimulate the production of angiogenic mediators, notably vascular endothelial growth factor (VEGF) [8,9]. Beyond the well-known angiogenic responses, recent studies indicate that hypoxia also engages multiple inflammatory and immune-regulatory pathways [10,11]. Hypoxia can alter cellular metabolic profiles, heighten inflammatory signaling, and influence immune cell activity, implying its involvement in PDR progression through complex molecular networks [12].

To address these gaps in knowledge, we applied a comprehensive bioinformatics strategy to identify and characterize hypoxia-related genes implicated in PDR. Using integrated approaches that combined differential expression analysis, weighted gene co-expression network construction, and machine learning-based feature selection, we profiled the hypoxia-associated molecular landscape of PDR and examined its links to immune microenvironment alterations. Our findings provide deeper insight into hypoxia-driven molecular mechanisms in PDR and highlight potential biomarkers for diagnosis and therapeutic intervention.

2. Method

2.1 Data acquisition and preprocessing

The gene expression dataset GSE146615 was obtained from the Gene Expression Omnibus (GEO) database and includes RNA sequencing data from 26 patients with proliferative diabetic retinopathy (PDR) and 21 healthy controls. Standard quality control procedures were applied to the raw expression data, followed by normalization.

To identify hypoxia-related genes (HRGs), we queried the GeneCards database (https://www.genecards.org/) using “Hypoxia” as the keyword and restricted the results to protein-coding genes. This search, performed on December 11, 2024, yielded 6,259 unique HRGs.

2.2 Differential gene expression analysis

We compared transcriptomic profiles between PDR and control groups using the limma package in R. Genes were considered differentially expressed if they satisfied the thresholds of $|\log_2$ fold change$| > 0$ and adjusted P-value < 0.05 (Benjamini–Hochberg correction). Volcano plots were generated to depict the overall distribution of significantly upregulated and downregulated genes.

2.3 Functional and pathway enrichment

GO enrichment analysis was performed to identify biological processes (BP), cellular components (CC), and molecular functions (MF) associated with PDR. KEGG pathway analysis was then used to explore potential disease-related pathways. All analyses were conducted with the clusterProfiler package in R and visualized as dot and bar plots.

2.4 Co-expression network construction

A weighted gene co-expression network was constructed to identify modules of co-expressed genes associated with PDR. The WGCNA package in R was employed, and the optimal soft-thresholding power (β) was selected by evaluating the scale-free topology criterion across β values from 1 to 20, targeting an $R^2 \geq 0.85$. Based on these criteria, $\beta = 11$ was chosen, balancing network scale-freeness and mean connectivity.

2.5 Hypoxia-related gene identification

To identify core PDR-associated genes, we performed intersection analysis between the DEGs identified from differential expression analysis and genes from the most PDR-relevant module identified by WGCNA. The resulting core genes were further intersected with a comprehensive database of hypoxia-related genes (n=6,259) to identify candidates specifically associated with hypoxic conditions. Venn diagrams were used to visualize these intersection analyses.

2.6 LASSO regression analysis

Least Absolute Shrinkage and Selection Operator (LASSO) regression with 10-fold cross-validation was applied to the hypoxia-related PDR genes to identify the most discriminative features for PDR diagnosis. The glmnet package in R was used for this analysis. LASSO coefficient paths were plotted to show how regression coefficients change with the regularization parameter lambda (λ).

The optimal λ value was determined using 10-fold cross-validation by plotting binomial deviance against log(λ). Two criteria were considered: lambda.min (minimum cross-validation error) and lambda.1se (1 standard error rule). The 1-SE criterion was used for final model selection to achieve optimal balance between model performance and parsimony.

2.7 XGBoost feature ranking

Extreme Gradient Boosting (XGBoost) was employed to validate and rank the importance of LASSO-selected genes using the xgboost package in R. Feature importance scores were calculated to assess the discriminative power of each gene in distinguishing PDR patients from healthy controls. Genes were ranked based on their importance scores, with the top-ranked genes selected for individual diagnostic performance evaluation.

2.8 Biomarker diagnostic evaluation

Receiver Operating Characteristic (ROC) curve analysis was performed to evaluate the diagnostic capability of the top four biomarkers identified via XGBoost, using the pROC package in R. The area under the curve (AUC) with corresponding 95% confidence intervals was calculated for each biomarker (PITRM1, DSC2, DSC3, and CXCL9) to determine their ability to distinguish PDR cases from healthy controls. Biomarkers with an AUC greater than 0.7 were considered to have acceptable diagnostic accuracy, and those with an AUC above 0.8 were regarded as having strong performance.

2.9 Immune cell infiltration analysis

The CIBERSORT algorithm was applied to estimate the relative abundance of 22 immune cell subsets in PDR patients (n = 26) and healthy controls (n = 21) based on bulk gene expression data. This method uses a deconvolution framework together with the LM22 leukocyte signature matrix to

infer immune cell composition.

Group comparisons for each immune cell type were conducted using appropriate statistical tests. Box plots were used to illustrate differences in immune cell proportions between the two cohorts, with statistical significance indicated as $P < 0.01$, $P < 0.05$, and "ns" for non-significant results. Additionally, a stacked bar plot was generated to depict the distribution of immune cell types in individual samples, with control samples shown on the left (blue) and PDR samples on the right (red).

2.10 Biomarker–immune cell correlations

Pearson correlation analysis was performed to investigate the relationships between the expression levels of the four top-ranked biomarker genes (CXCL9, DSC2, DSC3, PITRM1) and immune cell infiltration proportions. Only correlations with $P < 0.05$ were considered statistically significant. Results were visualized using dot plots, where dot size indicated correlation strength and color intensity represented statistical significance level.

2.11 Statistical Analysis

All statistical procedures were carried out in R (version 4.0 or later). For continuous variables, comparisons between groups were performed using either the Wilcoxon rank-sum test or Student's t-test, as appropriate. The Benjamini–Hochberg method was applied to control the false discovery rate for multiple comparisons. A threshold of $P < 0.05$ was considered statistically significant. Data analyses employed the following R packages: limma (differential expression), clusterProfiler (functional enrichment), WGCNA (co-expression network), glmnet (LASSO regression), xgboost (gradient boosting), pROC (ROC analysis), and e1071 (CIBERSORT). Data visualization was performed using ggplot2, ComplexHeatmap, and other relevant R packages.

3. Results

3.1 Differentially expressed genes in PDR

To explore transcriptional alterations linked to proliferative diabetic retinopathy, we analyzed the GSE146615 dataset, which contains expression profiles from 26 PDR patients and 21 healthy controls. Using thresholds of $|\log_2 FC| > 0$ and adjusted $P < 0.05$, we identified 1,650 differentially expressed genes (DEGs) (Figure 1A). Of these, 939 were upregulated and 711 were downregulated in the PDR group compared with controls.

3.2 KEGG pathway enrichment

Figure 1B shows that DEGs were enriched in pathways related to immune regulation, vascular function, and infection. The most represented pathways included phagosome, vascular smooth muscle contraction, rheumatoid arthritis, type I diabetes mellitus, and viral myocarditis, along with intestinal immune network for IgA production, allograft rejection, and viral life cycle.

3.3 GO functional enrichment

Figure 1C shows that DEGs were enriched in key biological processes such as small GTPase–mediated signal transduction, macroautophagy, and MHC protein complex assembly. In the cellular component category, enrichment was observed in secretory granule membrane, transport vesicle membrane, and MHC protein complexes. For molecular functions, the top terms included GTPase regulator activity, nucleoside-triphosphatase regulator activity, aminoacyltransferase activity, and

various ubiquitin-related transferase activities.

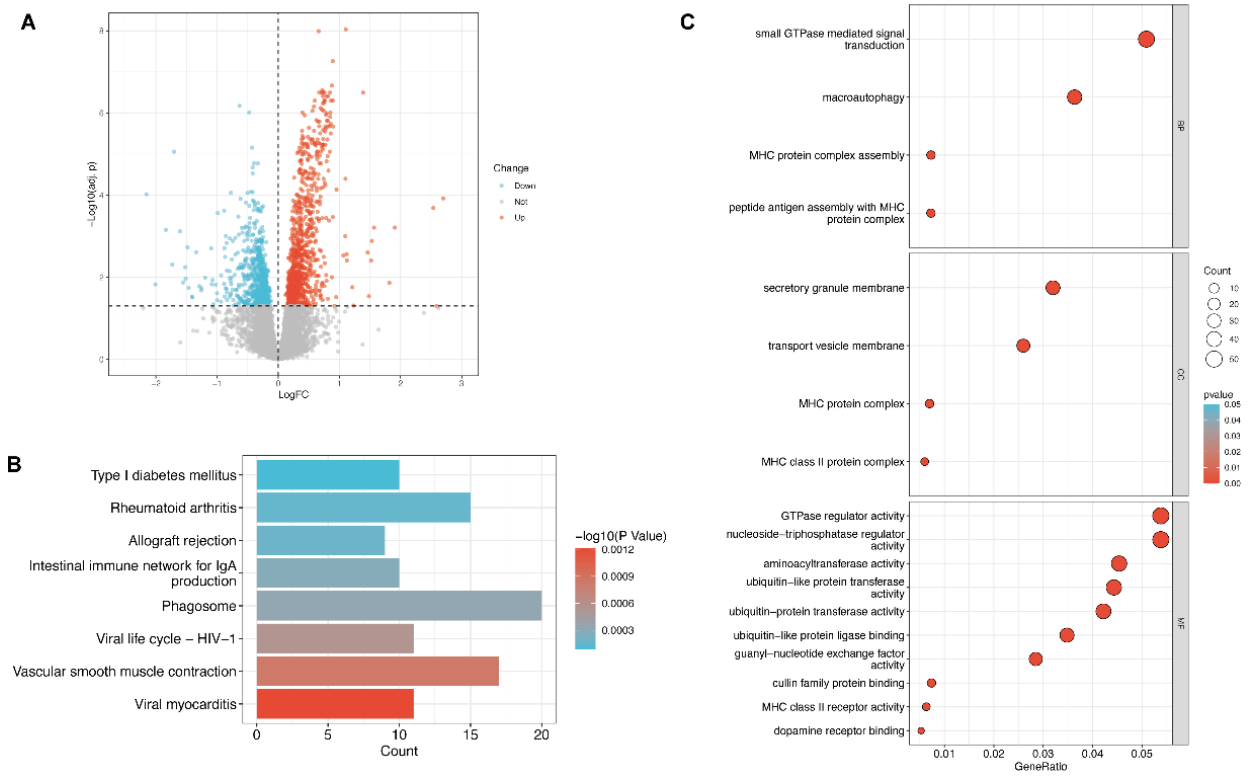

Figure 1: Overview of differential expression and functional enrichment analyses in proliferative diabetic retinopathy

(A) Volcano plot of 1,650 DEGs between PDR (n = 26) and controls (n = 21); red = upregulated (n = 939), blue = downregulated (n = 711) ($|\log_2 FC| > 0$, adjusted $P < 0.05$). (B) KEGG enrichment showing top pathways; bar length = gene count, color = $-\log_{10}$(P value). (C) GO enrichment for biological processes (BP), cellular components (CC), and molecular functions (MF); dot size = gene count, color = significance.

3.4 Co-expression network and module associations

To identify gene modules associated with proliferative diabetic retinopathy (PDR), we applied weighted gene co-expression network analysis (WGCNA) to the GSE146615 dataset. Prior to network construction, hierarchical clustering of samples was performed to detect potential outliers (Figure 2D). The dendrogram showed a clear separation between PDR and control samples, with no obvious outliers, indicating high data quality for subsequent analysis.

The optimal soft-thresholding power (β) was determined by assessing scale independence and mean connectivity (Figure 2E). A power of $\beta = 11$ satisfied the scale-free topology criterion ($R^2 > 0.8$) while maintaining low mean connectivity, ensuring a biologically meaningful network structure.

Gene clustering using a dynamic tree-cutting algorithm identified several distinct co-expression modules, each assigned a unique color (Figure 2A). Hierarchical clustering of module eigengenes (Figure 2C) revealed three major module groups: (1) MEblue and MEturquoise, which were highly similar, suggesting strongly correlated expression patterns; (2) MEbrown and MEyellow, which clustered together, indicating potential functional relatedness; and (3) MEgreen, MEblack, and MEred forming a tight subcluster, with MEgrey remaining more independent.

Module–trait correlation analysis (Figure 2B) identified MEbrown as the most relevant to PDR,

showing a strong negative correlation ($r = –0.82$, $P = 1.2\times10^{-12}$), indicating that genes in this module were markedly downregulated in PDR patients. MEgreen ($r = 0.42$, $P = 0.00307$) and MEblack ($r = 0.46$, $P = 0.00123$) showed significant positive correlations with PDR, while other modules exhibited weaker or non-significant associations. These findings highlight MEbrown, MEgreen, and MEblack as key modules potentially involved in PDR pathogenesis.

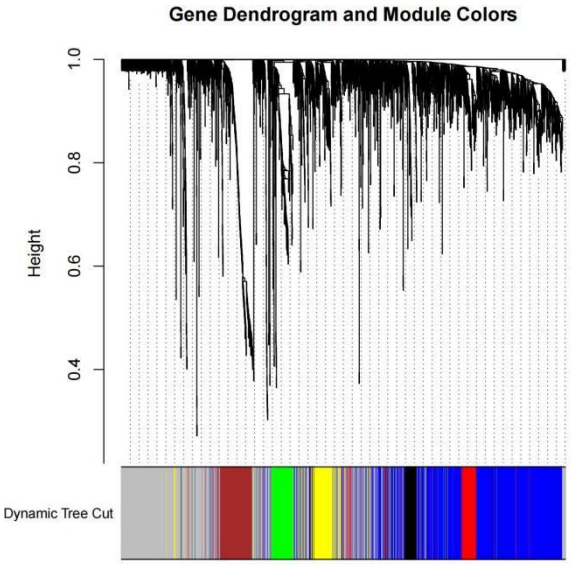

(A)

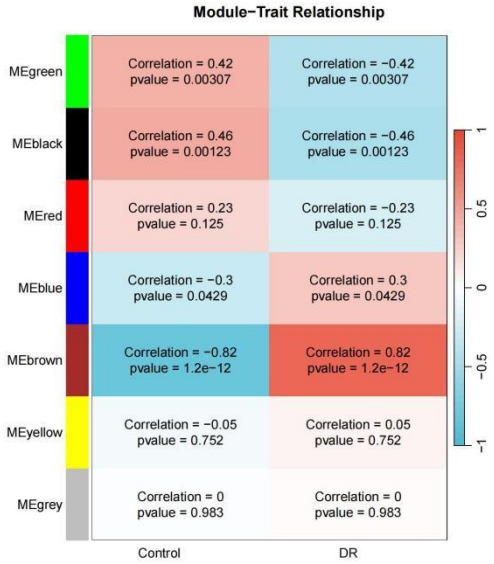

(B)

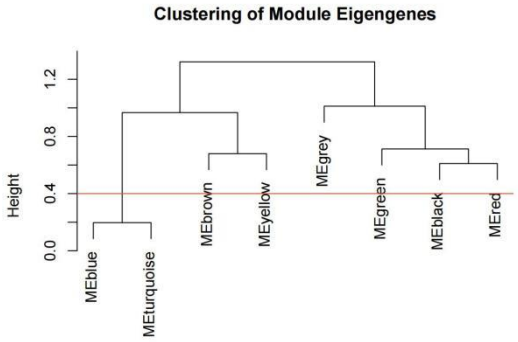

(C)

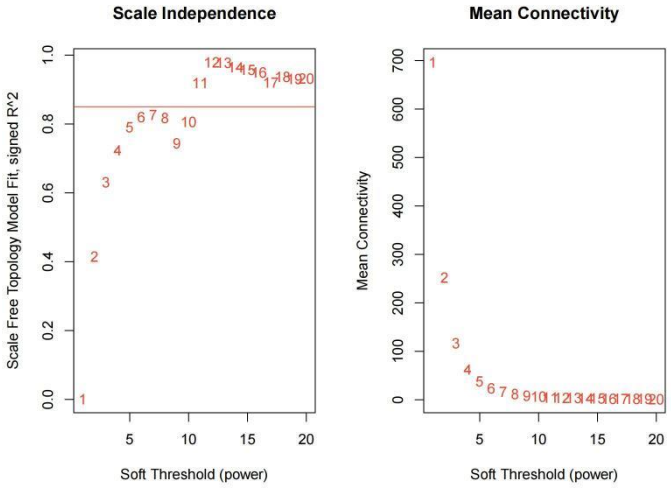

(E)

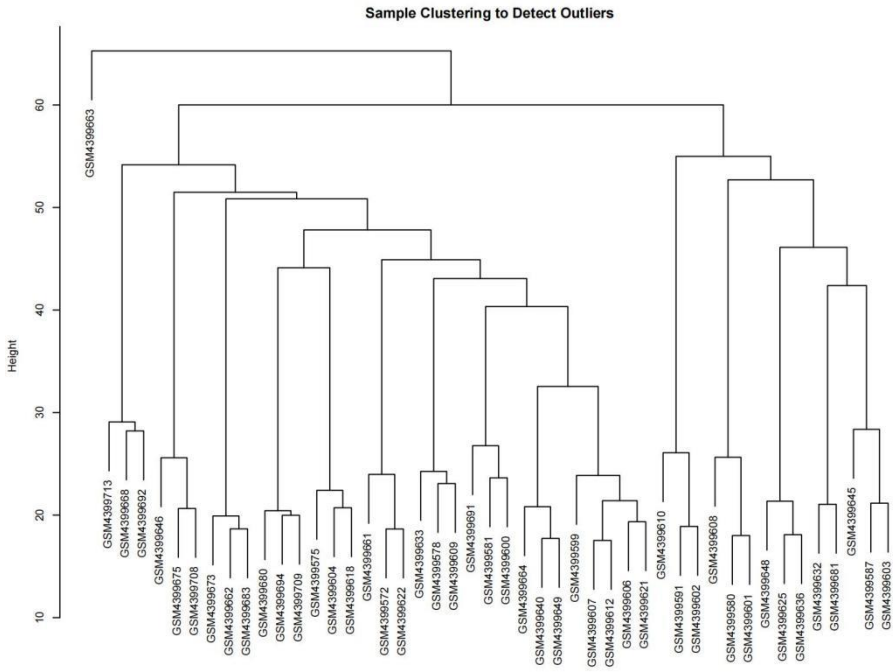

(D)

Figure 2: Weighted gene co-expression network analysis (WGCNA) identifies PDR-associated gene modules.

(A) Gene dendrogram and module identification. Seven modules were identified: turquoise, blue, brown, yellow, green, red, and black, with grey representing unassigned genes. (B) Module-trait relationship heatmap. The brown module shows strongest negative correlation with PDR ($r = -0.82$, $P = 1.2\times10^{-12}$), while green and black modules show positive correlations. (C) Hierarchical clustering of module eigengenes showing three main clusters at height threshold 0.4. (D) Sample clustering dendrogram showing clear separation between PDR patients and controls. Sample GSM4366605 shows potential outlier behavior but was retained. (E) Soft-thresholding power selection. $\beta = 11$ was selected as optimal based on scale-free topology criteria.

3.5 Core gene identification

To identify the most biologically relevant genes associated with PDR pathogenesis, we performed an integrative analysis combining our differential gene expression results with the WGCNA-derived gene modules. We intersected the 1,650 DEGs identified from our differential expression analysis with the 147 genes from the brown module (the most PDR-relevant module identified by WGCNA) (Figure 3A). This intersection yielded 34 core genes that are both significantly differentially expressed in PDR and co-expressed within the most disease-relevant gene module.

3.6 Hypoxia-related gene validation

Given our hypothesis that hypoxia is a critical driving factor in PDR development, we further refined our gene set by intersecting the 34 core PDR-associated genes with a comprehensive database of hypoxia-related genes (Figure 3B). This analysis identified 13 genes that are simultaneously differentially expressed in PDR, co-expressed in the disease-relevant brown module, and functionally associated with hypoxic conditions.

3.7 Selection of diagnostic genes using LASSO regression

To validate the differential expression patterns of the 13 identified hypoxia-related PDR genes, we performed comprehensive expression comparison analysis between PDR patients and healthy controls (Figure 3C). The box plot analysis revealed that 11 out of 13 genes showed statistically significant differential expression between the two groups. Specifically, PITRM1, TNK2, SESN3, DSC3, PTPN13, HEY2, CXCL9, and DSC2 demonstrated highly significant differences ($P < 0.001$), while PDLIM3, SH3BGRL2, and PTGER4 showed moderate significance ($P < 0.05$). Notably, KCNMB1 showed a trend toward significance, and only OTP did not reach statistical significance. The majority of genes showed consistent downregulation in PDR patients compared to controls, which aligns with the negative correlation observed for the brown module in our WGCNA analysis.

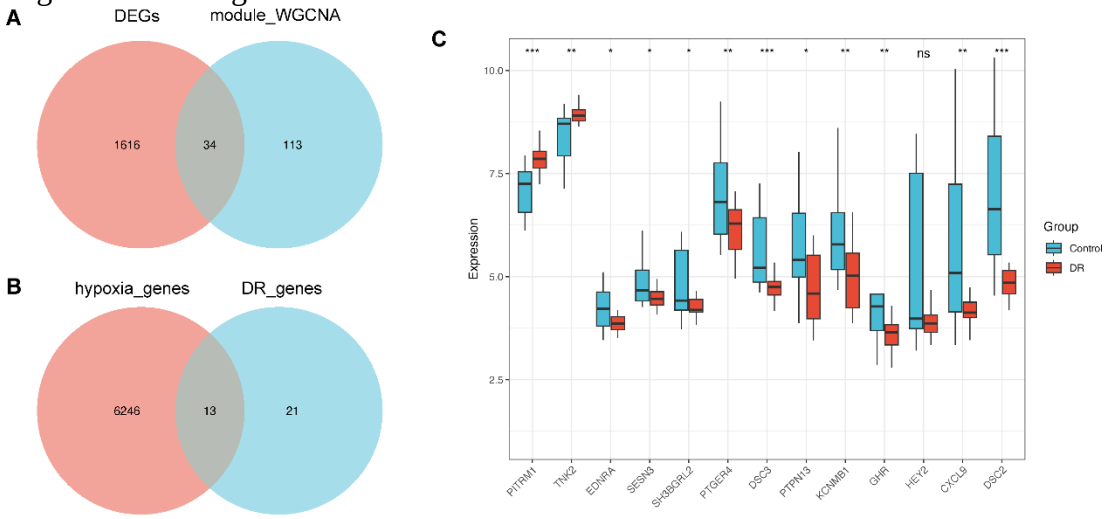

Figure 3: Integration analysis identifies hypoxia-related genes associated with PDR development

(A) Venn diagram showing intersection between DEGs (n=1,650) and brown module genes (n=147), yielding 34 core genes. (B) Venn diagram showing intersection between hypoxia genes (n=6,259) and core PDR genes (n=34), identifying 13 hypoxia-related PDR genes. (C) Box plots comparing expression of 13 genes between controls (blue, n=21) and PDR patients (red, n=26). Statistical significance: *** $P < 0.001$; ** $P < 0.01$; * $P < 0.05$; ns = not significant.

3.8 Selection of diagnostic genes using LASSO regression

To pinpoint the most informative genes for PDR diagnosis among the 13 hypoxia-related candidates, we applied the Least Absolute Shrinkage and Selection Operator (LASSO) method with tenfold cross-validation. This regularization approach efficiently selects relevant predictors by applying L1 penalties, thereby minimizing overfitting while preserving predictive performance.

We first examined the coefficient paths of all 13 genes across different values of the regularization parameter lambda (λ) (Figure 4A). The coefficient profile plot demonstrates how the regression coefficients of individual genes change as the penalty parameter increases. As log(λ) increases from left to right, the coefficients gradually shrink toward zero, with different genes being eliminated at different lambda values.

The optimal lambda parameter was determined using tenfold cross-validation, plotting binomial deviance against log(λ) (Figure 4B). The curve identified two vertical dashed lines: one for the lambda minimizing the cross-validation error (lambda.min) and another for the 1-SE lambda (lambda.1se), which favors a simpler model within one standard error of the minimum.

The final LASSO model selection results are presented through both coefficient visualization and importance ranking (Figure 4C-D). The dot plot shows the Mean Decrease Gini values for each of the 13 genes, which measures the contribution of each gene to node purity in the classification model (Figure 4C). DSC2 demonstrates the highest Mean Decrease Gini value (around 3.5), indicating its strongest discriminative power for PDR classification, followed by PITRM1, GHR, DSC3, CXCL9, and EDNRA with progressively lower but still substantial contributions. The remaining genes (KCNMB1, SESN3, HEY2, TNK2, PTGER4, SH3BGRL2, and PTPN13) showed lower Mean Decrease Gini values, suggesting reduced importance in the classification model.

To further evaluate feature importance, we applied XGBoost algorithm to rank the selected genes based on their contribution to the classification model (Figure 4D). The feature importance plot reveals DSC2 as the most important gene, followed by PITRM1, CXCL9, DSC3, and GHR. The remaining genes (HEY2, SH3BGRL2, PTPN13, EDNRA, SESN3, and KCNMB1) showed minimal importance scores below 0.05, suggesting that the top 5 genes constitute the core biomarker panel for PDR diagnosis. This dual analytical approach consistently identifies DSC2, PITRM1, CXCL9, DSC3, and GHR as the most critical hypoxia-related genes for PDR classification.

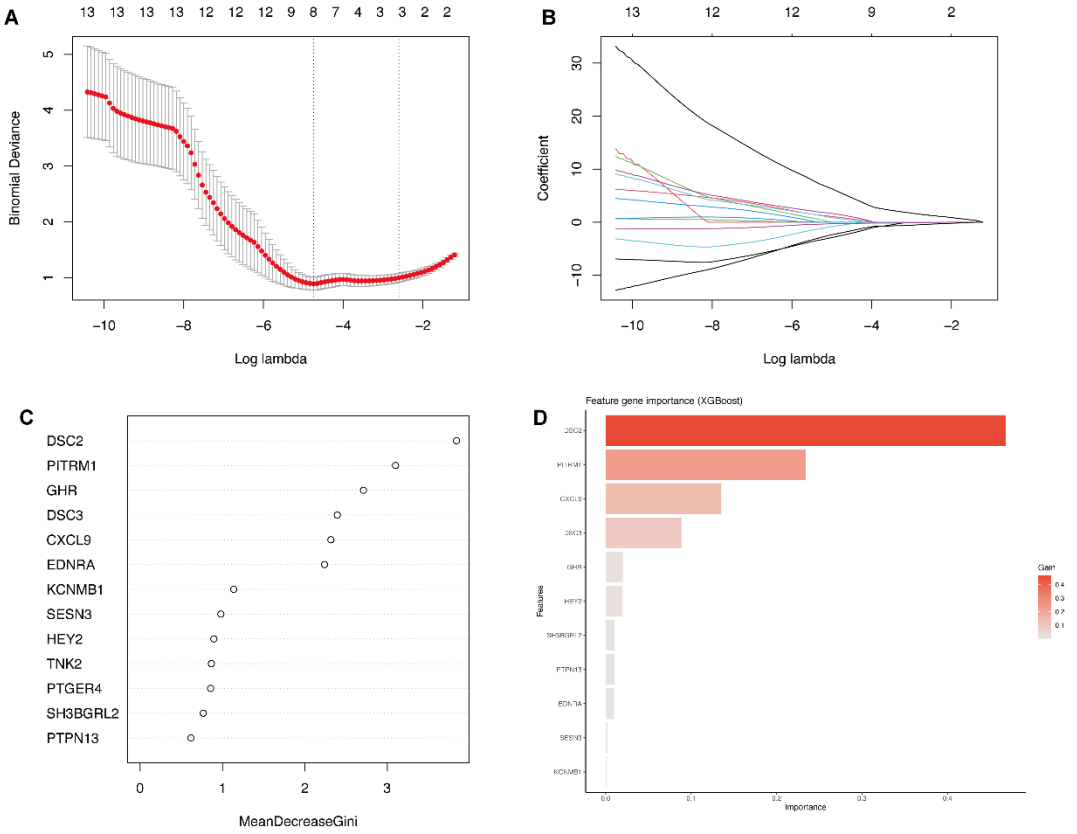

Figure 4: Machine learning-based feature selection and importance ranking of hypoxia-related PDR genes

(A) LASSO coefficient paths showing how gene coefficients change with regularization parameter log(λ). Numbers at top indicate remaining features at each lambda value. (B) 10-fold cross-validation curve for optimal lambda selection. Vertical dashed lines indicate lambda.min and lambda.1se values. (C) Mean Decrease Gini analysis showing gene contribution to classification model node purity. DSC2 shows highest value (~3.5). (D) XGBoost feature importance ranking. DSC2 demonstrates highest importance (0.4), followed by PITRM1 (0.25), CXCL9 (0.15), DSC3 (0.1), and GHR (0.05),

establishing the core biomarker panel for PDR diagnosis.

3.9 Diagnostic performance of biomarkers

To assess the diagnostic utility of the top-selected genes, we performed ROC curve analysis (Figure 5). PITRM1 achieved the highest AUC (0.863, 95% CI: 0.76–0.965), indicating strong discriminative capacity. DSC2 showed comparable performance (AUC = 0.861, 95% CI: 0.746–0.972). DSC3 also demonstrated high accuracy (AUC = 0.837, 95% CI: 0.722–0.952), while CXCL9 exhibited moderate but significant predictive power (AUC = 0.749, 95% CI: 0.594–0.904). All four exceeded the AUC threshold of 0.7, with three surpassing 0.8.

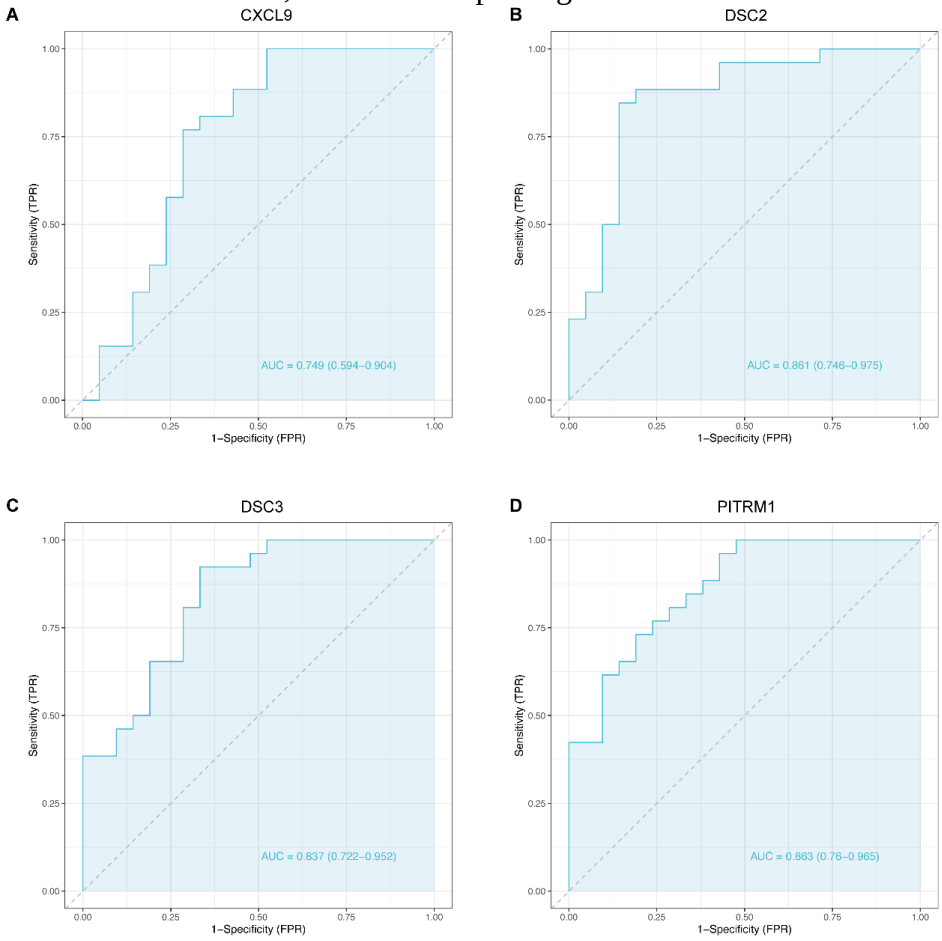

Figure 5: Individual biomarker ROC performance analysis

(A) CXCL9 ROC curve: AUC = 0.749 (0.594-0.904). (B) DSC2 ROC curve: AUC = 0.861 (0.746-0.975). (C) DSC3 ROC curve: AUC = 0.837 (0.722-0.952). (D) PITRM1 ROC curve: AUC = 0.863 (0.76-0.965). All biomarkers demonstrate significant diagnostic potential for distinguishing PDR patients from controls.

3.10 Immune cell infiltration in PDR

To investigate the immune microenvironment changes associated with PDR development, we performed immune cell infiltration analysis using the CIBERSORT algorithm. This analysis estimated the relative proportions of 22 distinct immune cell types in both PDR patients and healthy controls. The comparative analysis revealed significant alterations in specific immune cell

populations between the two groups (Figure 6A). Among the 22 immune cell types analyzed, three showed statistically significant differences between PDR and control groups. Specifically, PDR patients demonstrated significantly increased infiltration of plasma cells ($P < 0.01$) and T cells CD8 ($P < 0.01$) compared to healthy controls. Conversely, PDR patients showed significantly decreased levels of mast cells resting ($P < 0.01$) relative to controls. The increased plasma cell infiltration suggests enhanced antibody production and humoral immune responses in PDR pathogenesis.

The stacked bar plot visualization of immune cell proportions across all individual samples revealed substantial heterogeneity in immune composition between patients (Figure 6B). Each vertical bar represents the complete immune profile of one sample, with different colors indicating various immune cell types according to the comprehensive legend. The analysis demonstrated clear differences in immune landscapes between control samples (left side, blue label) and PDR samples (right side, red label). PDR patients generally showed altered patterns of immune cell distribution, with notable increases in B cell populations and plasma cells, consistent with the statistical analysis.

3.11 Biomarker–immune cell associations

We examined the associations between the four key biomarkers and immune cell composition (Figures 6C–F). CXCL9 showed a strong positive correlation with activated CD4 memory T cells, consistent with its chemokine-mediated role in T cell recruitment. DSC3 exhibited negative correlations with follicular helper T cells, resting mast cells, and eosinophils, suggesting involvement in regulating specific immune responses. DSC2 was positively correlated with regulatory T cells, resting NK cells, M2 macrophages, and activated dendritic cells, pointing to a role in immune modulation and tissue homeostasis. PITRM1 correlated positively with plasma cells and moderately with activated CD4 memory T cells, but negatively with resting NK cells.

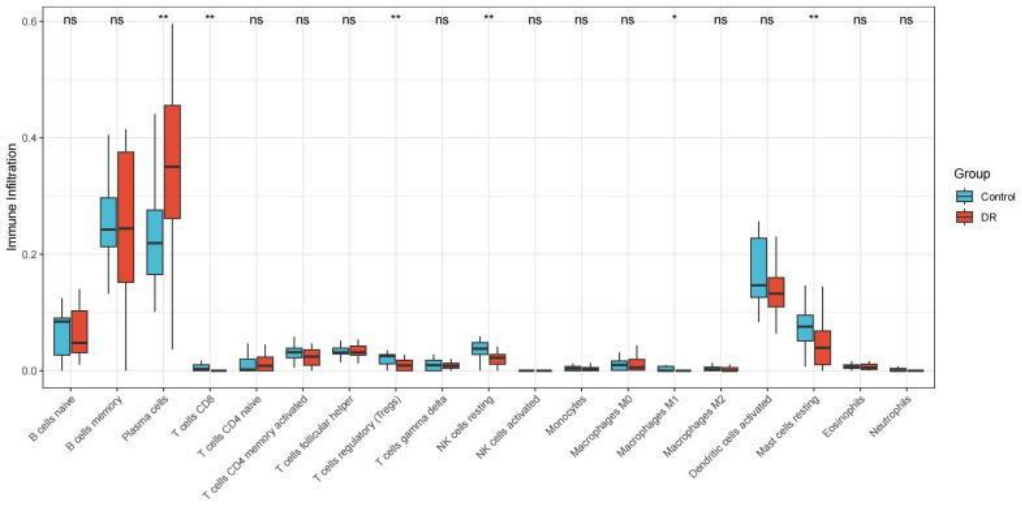

(A)

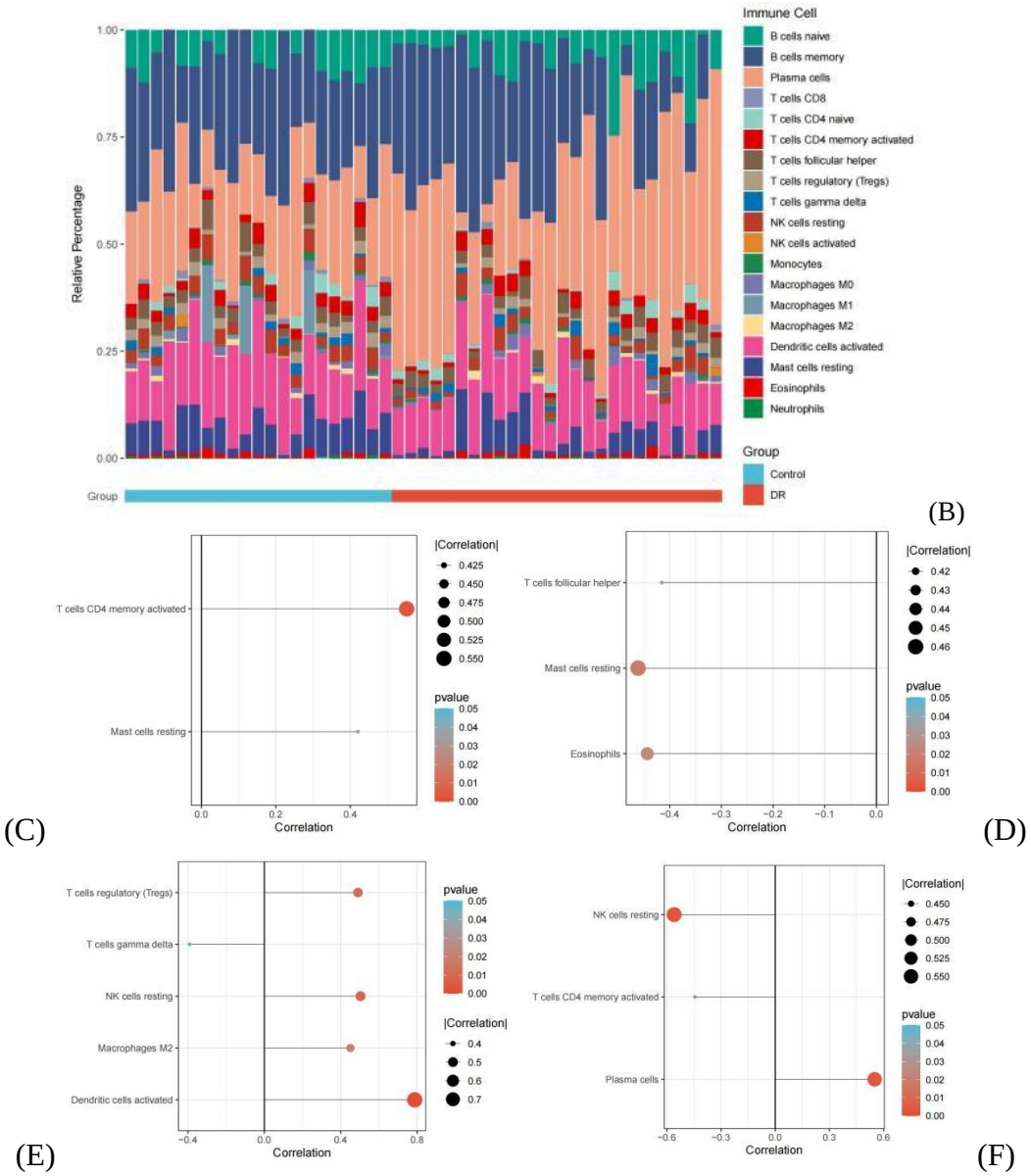

Figure 6: Immune infiltration analysis reveals altered immune landscape and biomarker-immune cell correlations in PDR

(A) Box plots comparing immune cell proportions between controls (blue, n=21) and PDR patients (red, n=26). Statistical significance: ** $P < 0.01$; * $P < 0.05$; ns = not significant. (B) Stacked bar plot showing immune cell composition across all samples. Controls (left) and PDR patients (right) show distinct patterns. (C-F) Correlation analysis between biomarkers and immune cells showing significant associations ($P < 0.05$). (C) CXCL9 correlations. (D) DSC3 correlations. (E) DSC2 correlations. (F) PITRM1 correlations. Dot size indicates correlation strength, color represents significance.

4. Conclusion

In this study, we applied a comprehensive transcriptomic approach to examine hypoxia-associated genes in proliferative diabetic retinopathy (PDR). By integrating differential gene expression profiling, weighted gene co-expression network construction, and machine learning-based feature

selection, we identified four candidate biomarkers—CXCL9, DSC2, DSC3, and PITRM1—significantly linked to PDR. Among them, CXCL9 was elevated, while DSC2, DSC3, and PITRM1 showed reduced expression. All four genes demonstrated notable correlations with patterns of immune cell infiltration.

CXCL9 encodes a chemokine induced by interferon-γ that mediates T cell recruitment through binding to the CXCR3 receptor. Elevated CXCL9 levels have been reported in the vitreous of PDR patients, and retinal endothelial cells can produce CXCL9 under inflammatory stimulation[13-14]. Our findings are consistent with these reports, and the upregulation observed here may reflect hypoxia-driven inflammatory activation in PDR. Given the known role of CXCL9 in leukocyte chemotaxis, its increased expression could be linked to the enhanced immune cell presence observed in PDR tissues[15-17]. Further studies will be required to determine whether CXCL9 directly contributes to pathological angiogenesis or is a secondary marker of inflammation.

DSC2 and DSC3 are members of the desmosomal cadherin family, which play a key role in cell–cell adhesion and maintaining tissue integrity [18-19] Although their specific functions in the retina have not been described, reduced expression of adhesion molecules has been associated with barrier dysfunction in other vascular beds under pathological conditions [20]. The downregulation of DSC2 and DSC3 in our dataset may indicate structural alterations in retinal endothelial junctions during PDR, potentially facilitating immune cell infiltration. This interpretation remains speculative and would need confirmation in experimental models assessing blood–retinal barrier function.

PITRM1 encodes a mitochondrial matrix metalloprotease that degrades targeting peptides and contributes to mitochondrial proteostasis[21]. While its role in retinal disease has not been reported, mitochondrial dysfunction is a recognized feature of diabetic retinal pathology [22]. The lower PITRM1 expression observed in our analysis may be associated with impaired mitochondrial quality control under hypoxic stress, potentially leading to increased oxidative damage[23-24]. These possibilities warrant further mechanistic studies to clarify whether PITRM1 downregulation is a cause or consequence of PDR progression.

Our results suggest that hypoxia in PDR may influence multiple biological processes, including immune cell recruitment, vascular adhesion, and mitochondrial homeostasis. CXCL9 appears to have a documented link to PDR inflammation, while DSC2, DSC3, and PITRM1 represent less explored candidates that could open new research directions.

This study has several limitations. First, our findings are based solely on transcriptomic data from a single dataset and require validation in independent cohorts and experimental systems. Second, the functions of DSC2, DSC3, and PITRM1 in retinal tissue are not yet established. Third, the cross-sectional nature of the data limits our ability to infer temporal changes or causality.

In conclusion, we identified four hypoxia-related genes associated with PDR, of which CXCL9 shows the strongest literature support for involvement in retinal inflammation, while DSC2, DSC3, and PITRM1 represent novel candidates for future study. These results expand the molecular landscape of hypoxia in PDR and may guide future efforts to develop diagnostic biomarkers and therapeutic targets.

References

[1] Miller DJ, Cascio MA, Rosca MG. Diabetic Retinopathy: The Role of Mitochondria in the Neural Retina and Microvascular Disease. Antioxidants (Basel). 2020 Sep 23;9(10):905.

[2] Pedrini A, Nowosielski Y, Rehak M. Diabetic retinopathy-recommendations for screening and treatment. Wien Med Wochenschr. 2025;175(9-10):253-263.

[3] Giuliari GP, Guel DA, Gonzalez VH. Pegaptanib sodium for the treatment of proliferative diabetic retinopathy and diabetic macular edema. Curr Diabetes Rev. 2009;5(1):33-38.

[4] Stewart MW. A Review of Ranibizumab for the Treatment of Diabetic Retinopathy. Ophthalmol Ther. 2017;6(1):33-47.

[5] Zhang P, Liu N, Wang Y. Insulin may cause deterioration of proliferative diabetic retinopathy. Med Hypotheses. 2009; 72(3):306-308.
[6] Stecker MM, Stevenson MR. Anoxia-induced changes in optimal substrate for peripheral nerve. Neuroscience. 284:653-667.
[7] Mudaliar S, Hupfeld C, Chao DL. SGLT2 Inhibitor-Induced Low-Grade Ketonemia Ameliorates Retinal Hypoxia in Diabetic Retinopathy-A Novel Hypothesis. J Clin Endocrinol Metab. 2021; 106(5):1235-1244.
[8] Büchler P, Reber HA, Büchler M, et al. Hypoxia-inducible factor 1 regulates vascular endothelial growth factor expression in human pancreatic cancer. Pancreas. 2003; 26(1):56-64.
[9] Liu LX, Lu H, Luo Y, et al. Stabilization of vascular endothelial growth factor mRNA by hypoxia-inducible factor 1. Biochem Biophys Res Commun. 2002; 291(4):908-914.
[10] Scholz CC, Taylor CT. Targeting the HIF pathway in inflammation and immunity. Curr Opin Pharmacol. 2013; 13(4):646-653.
[11] Mamlouk S, Wielockx B. Hypoxia-inducible factors as key regulators of tumor inflammation. Int J Cancer. 2013; 132(12):2721-2729.
[12] Arjamaa O, Pöllönen M, Kinnunen K, Ryhänen T, Kaarniranta K. Increased IL-6 levels are not related to NF-κB or HIF-1α transcription factors activity in the vitreous of proliferative diabetic retinopathy. J Diabetes Complications. 2011 Nov-Dec; 25(6):393-397.
[13] Müller M, Carter S, Hofer MJ, Campbell IL. Review: The chemokine receptor CXCR3 and its ligands CXCL9, CXCL10 and CXCL11 in neuroimmunity--a tale of conflict and conundrum. Neuropathol Appl Neurobiol. 2010;36(5):368-387.
[14] Xu Y, Cheng Q, Yang B, et al. Increased sCD200 Levels in Vitreous of Patients With Proliferative Diabetic Retinopathy and Its Correlation With VEGF and Proinflammatory Cytokines. Invest Ophthalmol Vis Sci. 2015;56(11):6565-6572.
[15] van der Aa LM, Chadzinska M, Golbach LA, Ribeiro CM, Lidy Verburg-van Kemenade BM. Pro-inflammatory functions of carp CXCL8-like and CXCb chemokines. Dev Comp Immunol. 2012; 36(4):741-750.
[16] Liu HX, Wang YY, Yang XF. Differential expression of plasma cytokines in sepsis patients and their clinical implications. World J Clin Cases. 2024; 12(25):5681-5696.
[17] Lo BK, Yu M, Zloty D, Cowan B, Shapiro J, McElwee KJ. CXCR3/ligands are significantly involved in the tumorigenesis of basal cell carcinomas. Am J Pathol. 2010; 176(5):2435-2446.
[18] Lee JYW, McGrath JA. Mutations in genes encoding desmosomal proteins: spectrum of cutaneous and extracutaneous abnormalities. Br J Dermatol. 2021; 184(4):596-605.
[19] Nie Z, Merritt A, Rouhi-Parkouhi M, Tabernero L, Garrod D. Membrane-impermeable cross-linking provides evidence for homophilic, isoform-specific binding of desmosomal cadherins in epithelial cells. J Biol Chem. 2011; 286(3):2143-2154.
[20] Soe HJ, Khan AM, Manikam R, Samudi Raju C, Vanhoutte P, Sekaran SD. High dengue virus load differentially modulates human microvascular endothelial barrier function during early infection. J Gen Virol. 2017; 98(12):2993-3007.
[21] Brunetti D, Catania A, Viscomi C, et al. Role of PITRM1 in Mitochondrial Dysfunction and Neurodegeneration. Biomedicines. 2021;9(7). Published 2021 Jul 17.
[22] Kowluru RA, Mohammad G, Santos JM, Tewari S, Zhong Q. Interleukin-1β and mitochondria damage, and the development of diabetic retinopathy. J Ocul Biol Dis Infor. 2011; 4(1-2):3-9.
[23] Guo Z, Tian Y, Liu N, et al. Mitochondrial Stress as a Central Player in the Pathogenesis of Hypoxia-Related Myocardial Dysfunction: New Insights. Int J Med Sci. 2024; 21(13):2502-2509.
[24] Xin T, Lv W, Liu D, Jing Y, Hu F. Opa1 Reduces Hypoxia-Induced Cardiomyocyte Death by Improving Mitochondrial Quality Control. Front Cell Dev Biol. 2020 Aug 28; 8: 853.